Title

Precision of Hole-Drilling Residual Stress Depth Profile Measurements and an Updated Uncertainty Estimator

Journal

Experimental Mechanics, 61(3)

ISSN

0014-4851

Authors

Olson, MD
DeWald, AT
Hill, MR

Publication Date

2021-03-01

DOI

10.1007/s11340-020-00679-1

Precision of hole-drilling residual stress depth profile measurements and an updated uncertainty estimator

M.D. Olson[1*], A.T. DeWald[1], and M.R. Hill[2]
[1]*Hill Engineering, LLC, 3083 Gold Canal Drive, Rancho Cordova, CA*
[2]*Department of Mechanical and Aerospace Engineering, University of California, One Shields Avenue, Davis, CA*

Submitted to *Experimental Mechanics, August 2020*
Accepted and Published, November 2020
https://doi.org/10.1007/s11340-020-00679-1

ABSTRACT

Background: Measurement precision and uncertainty estimation are important factors for all residual stress measurement techniques. The values of these quantities can help to determine whether a particular measurement technique would be viable option. **Objective**: This paper determines the precision of hole-drilling residual stress measurement using repeatability studies and develops an updated uncertainty estimator. **Methods**: Two repeatability studies were performed on test specimens extracted from an aluminum and titanium shot peened plate. Each repeatability study included 12 hole-drilling measurements performed using a bespoke automated milling machine. Repeatability standard deviations were determined for each population. The repeatability studies were replicated using a commercially available manual hole-drilling milling machine (RS-200, Micro-Measurements). An updated uncertainty estimator was developed and was assessed using an acceptance criterion. The acceptance criterion compared an expected percentage of points (68%) to the fraction of points in the stress versus depth profile where the measured stresses ± its total uncertainty contained the mean stress of the repeatability studies. **Results**: Both repeatability studies showed larger repeatability standard deviations at the surface that decay quickly (over about 0.3 mm). The repeatability standard deviation was significantly smaller in

*Corresponding author, Tel: (916) 635-5706, Fax: (916) 604-4517
E-mail address: molson@hill-engineering.com

the aluminum plate (max ≈ 15 MPa, RMS ≈ 6.4 MPa) than in the titanium plate (max ≈ 60 MPa, RMS ≈ 21.0 MPa). The repeatability standard deviations were significantly larger when using the manual milling machine in the aluminum plate (RMS ≈ 21.7 MPa), and for the titanium plate (RMS ≈ 18.9 MPa). **Conclusions**: The single measurement uncertainty estimate met a defined acceptance criterion based on the confidence interval of the uncertainty estimate.

Keywords: Residual stress, uncertainty, hole-drilling, precision, repeatability, regularization

TABLE OF SYMBOLS

$\bar{\mathbf{a}}$, $\bar{\mathbf{b}}$	Numerical calibration coefficient matrices
$\boldsymbol{p}$, $\boldsymbol{q}$, $\boldsymbol{t}$	Strain invariant vectors
$\boldsymbol{P}$, $\boldsymbol{Q}$, $\boldsymbol{T}$	Stress invariant vectors
N	Number of rows in the invariant vectors
ν	Poisson's ratio
E	Elastic modulus
ε	Measured strain
$\bar{z}$	Average cut depth
h	Cut depth
σ	Normal stress
τ	Shear stress
β	Regulation parameter
C	penalization matrix
α	Regulation parameter
$\hat{\boldsymbol{p}}, \hat{\boldsymbol{q}}$, and $\hat{\boldsymbol{t}}$	Fitted strain invariants
$\mathbf{U}_{\sigma,\varepsilon}$	Stress uncertainty from strain uncertainty
$\boldsymbol{U}_{\varepsilon}$	Strain uncertainty
e	Lower limit of strain uncertainty
$\boldsymbol{U}_{\sigma,\mathrm{reg}}$	Stress uncertainty from regularization uncertainty
$\boldsymbol{U}_{\sigma,\mathrm{tot}}$	Total stress uncertainty
p_{std}, q_{std}, t_{std}	"Standard errors" in the strain invariants
p_{rms}, q_{rms}, t_{rms}	Mean squares of the misfit strain vectors

1. INTRODUCTION

Precision is an important parameter to consider when selecting a measurement technique since it provides the expected measurement variability for a given test method. The definition of precision is the closeness of agreement between independent test results obtained under stipulated conditions and is closely related to measurement repeatability. Repeatability is the precision where the stipulated

conditions require that the same test method is applied to identical test specimens, in the same laboratory, by the same operator, over a short interval of time [1]. Repeatability is quantified by the repeatability standard deviation, which is simply the standard deviation of test results from a repeatability study.

The precision of a measurement does not quantify the measurement accuracy, which is determined by comparing the closeness of a test result to an accepted reference standard [1]. There are no perfect reference standards available for residual stress measurements, which limits quantification of residual stress measurement accuracy. Inter-method comparisons are often used to provide insight into measurement accuracy [2,3,4,5] as well as experiments on specimens having an expected residual stress field found from an analytical model [6,7]. This paper is intended to address measurement repeatability, not measurement accuracy.

The repeatability of hole-drilling has been determined in a prior publication for near-zero residual stress, using stress relieved specimens in AISI 1018 carbon-steel and 304 stainless steel [8]. The repeatability standard deviation was 14 MPa for the carbon steel specimens and 12 MPa for the stainless steel specimens under the assumption that the stress was constant with depth. The study included a cautionary note stating that measurements in specimens with non-zero residual stresses would be expected to exhibit larger variability compared to unstressed samples and that the variability would be larger if the study had assessed residual stress as a function of depth (i.e., a residual stress versus depth profile) instead of constant stress as assumed in the prior study.

The reproducibility of hole-drilling was also studied in a prior publication using shot peened steel specimens and friction stir welded aluminum specimens [9]. A reproducibility experiment is similar to a repeatability experiment, except that measurements are performed at different laboratories rather than at one laboratory. The hole-drilling measurements in [9] determined residual stress as a function of depth.

The study reported stress versus depth profiles for only some of the participating laboratories at only some cut depths, but omitted reporting the reproducibility standard deviations. The reproducibility standard deviation was estimated to be around 40 MPa for the friction stir welded aluminum specimens and several hundred MPa for the shot peened steel specimens. Data for both specimen types had higher stress standard deviation of stress at shallow depth (0.02 to 0.2 mm) than was found 1 mm below the surface (the nominal hole diameter was 2 mm).

The primary objective of the present study is to establish precision for hole-drilling when assessing typical residual stress versus depth profiles. Additionally, the present study develops an improved uncertainty estimate for hole-drilling. Lastly, the precision of hole-drilling will be compared between two different hole-drilling machines, where one is a bespoke automated machine and the other is a commercially available manual machine (RS-200, Micro-Measurements [10]).

2. METHODS

2.1. Overview

Hole-drilling repeatability is assessed in two different configurations: a shot peened aluminum plate and a shot peened titanium plate. Each repeatability assessment includes 12 hole-drilling measurements and a statistical analysis to determine the repeatability standard deviation for each set. Each set of measurements is performed on the same plate. The description of each specimen is provided later.

2.2. Hole-drilling measurement

A useful summary of the theoretical background for hole-drilling is given in [11] and the technique is standardized in ASTM E837-13 [8]. Key details are summarized here to provide context needed to establish the improved uncertainty estimator. Hole-drilling (also known as incremental center hole-drilling) involves drilling a small hole in a test specimen in small increments of depth, h_1, h_2, …, h_N. The removal of stressed material causes deformation as the initial residual stresses are redistributed.

Deformation is recorded after each material removal step using a strain gage rosette located near the hole on the surface of the specimen. The recorded strain versus depth data are then used to compute the stress versus depth profile present prior to hole-drilling.

The stress computation uses numerical calibration coefficient matrices $\bar{\mathbf{a}}$ and $\bar{\mathbf{b}}$ (also known as compliance matrices) that relate the strains measured at the strain gage locations to those that would be measured for a chosen set of stress basis functions. The stress basis functions used here (and in ASTM E837-13) are unit pulses. The numerical coefficients are computed using an elastic finite element calculation as described in [12,13]. The $\bar{\mathbf{a}}$ calibration coefficient matrix provides the strain at each cut depth that would be caused for a unit magnitude mean equibiaxial stress (i.e., $\sigma_{xx} = \sigma_{yy} = 1$) applied to the hole boundary over each cut depth increment and the $\bar{\mathbf{b}}$ calibration matrix provides the strain that would be caused for a unit magnitude mean shear stress (i.e., $\tau_{xy} = 1$) applied to the hole boundary. The $\bar{\mathbf{a}}$ and $\bar{\mathbf{b}}$ calibration coefficient matrices are formed by applying the loading described above for each cut depth increment (for each cut depth), determining strain, and forming a lower triangular matrix of dimension N x N, where N is the number of cut depth increments. ASTM E837-13 provides a tabulation of $\bar{\mathbf{a}}$ and $\bar{\mathbf{b}}$ for various strain gage designs.

With the compliance matrices known, the in-plane stresses can be calculated using the constitutive equation

$$\begin{aligned} \bar{\mathbf{a}}\boldsymbol{P} &= \frac{E}{1+\nu}\boldsymbol{p}, \\ \bar{\mathbf{b}}\boldsymbol{Q} &= E\boldsymbol{q}, \\ \bar{\mathbf{b}}\boldsymbol{T} &= E\boldsymbol{t} \end{aligned} \tag{1}$$

where $\boldsymbol{p}$, $\boldsymbol{q}$, and $\boldsymbol{t}$ are strain invariant vectors and $\boldsymbol{P}$, $\boldsymbol{Q}$, and $\boldsymbol{T}$ are stress invariant vectors having N rows, one for each cut depth increment [8]. Strain invariants are combinations of strains at different clock positions around the hole, with elements

$$\begin{aligned} p_i &= \left(\varepsilon_{0_i^\circ} + \varepsilon_{90_i^\circ}\right)/2, \\ q_i &= \left(\varepsilon_{90_i^\circ} - \varepsilon_{0_i^\circ}\right)/2, \\ t_i &= \left(\varepsilon_{0_i^\circ} + \varepsilon_{90_i^\circ} - 2\varepsilon_{225_i^\circ}\right)/2 \end{aligned} \tag{2}$$

Stress invariant vectors have one row for each average depth increment, $\bar{z}_i = (h_i + h_{i-1})/2$. They are linear combinations of the stress components with elements defined as

$$\begin{aligned} P_i &= \left(\sigma_{xx_i} + \sigma_{yy_i}\right)/2, \\ Q_i &= \left(\sigma_{yy_i} - \sigma_{xx_i}\right)/2, \\ T_i &= \tau_{xy_i}\,. \end{aligned} \tag{3}$$

The above constitutive equations inherently assume there is no noise in the measured strain data, and noise is known to cause erroneous, large stress gradients in the calculated stresses [14]. To smooth out noise in the strain data, Tikhonov regularization is added to Eq. (1) and changes the constitutive equations to

$$\begin{aligned} (\bar{\mathbf{a}}^{\mathbf{T}}\bar{\mathbf{a}} + \beta_P \mathbf{C}^{\mathbf{T}}\mathbf{C})\boldsymbol{P} &= \frac{E}{1+\nu}\bar{\mathbf{a}}^{\mathbf{T}}\boldsymbol{p}, \\ \left(\bar{\mathbf{b}}^{\mathbf{T}}\bar{\mathbf{b}} + \beta_Q \mathbf{C}^{\mathbf{T}}\mathbf{C}\right)\boldsymbol{Q} &= E\bar{\mathbf{b}}^{\mathbf{T}}\boldsymbol{q}, \\ \left(\bar{\mathbf{b}}^{\mathbf{T}}\bar{\mathbf{b}} + \beta_T \mathbf{C}^{\mathbf{T}}\mathbf{C}\right)\boldsymbol{T} &= E\bar{\mathbf{b}}^{\mathbf{T}}\boldsymbol{t} \end{aligned} \tag{4}$$

where **C** is a matrix that penalizes the second derivative of the stress solution [8]. The matrix **C** consists of zeros in the first and last rows and a tridiagonal structure for the other rows (i = 2, N-1). The tridiagonal entries for row i are computed from depths as

$$\frac{-2}{(h_{i+1}-h_{i-1})(h_i-h_{i-1})}, \frac{2}{(h_i-h_{i-1})(h_{i+1}-h_i)}, \frac{-2}{(h_{i+1}-h_i)(h_{i+1}-h_{i-1})}. \tag{5}$$

Scalar parameters β (β_P, β_Q, β_T in Eq. (4)) determine the amount of regularization used. Often in practice, values of β can be very small (~10^{-15}) and can vary significantly. For clarity, in this work β is defined in terms of a new regularization parameter α (α_P, α_Q, α_T), via

$$\begin{aligned} \beta_P &= 10^{\alpha_P}, \\ \beta_Q &= 10^{\alpha_Q}, \\ \beta_T &= 10^{\alpha_T}. \end{aligned} \tag{6}$$

The above provides a means for computing the stress invariant versus depth vectors $\boldsymbol{P}$, $\boldsymbol{Q}$, and $\boldsymbol{T}$ given vectors of strain invariant versus depth data, $\boldsymbol{p}$, $\boldsymbol{q}$, and $\boldsymbol{t}$ and specific values of α

$$\begin{aligned} \boldsymbol{P} &= \boldsymbol{V_P p}, \\ \boldsymbol{Q} &= \boldsymbol{V_Q q}, \\ \boldsymbol{T} &= \boldsymbol{V_T t} \end{aligned} \tag{7}$$

where

$$\begin{aligned} \boldsymbol{V_P} &= (\bar{\mathbf{a}}^{\mathbf{T}}\bar{\mathbf{a}} + \beta_P \mathbf{C}^{\mathbf{T}}\mathbf{C})^{-\mathbf{1}} \left(\frac{E}{1+\nu}\right) \bar{\mathbf{a}}^{\mathbf{T}}, \\ \boldsymbol{V_Q} &= \left(\bar{\mathbf{b}}^{\mathbf{T}}\bar{\mathbf{b}} + \beta_Q \mathbf{C}^{\mathbf{T}}\mathbf{C}\right)^{-\mathbf{1}} E\bar{\mathbf{b}}^{\mathbf{T}}, \\ \boldsymbol{V_T} &= \left(\bar{\mathbf{b}}^{\mathbf{T}}\bar{\mathbf{b}} + \beta_T \mathbf{C}^{\mathbf{T}}\mathbf{C}\right)^{-\mathbf{1}} E\bar{\mathbf{b}}^{\mathbf{T}} \end{aligned} \tag{8}$$

Given the stress invariant versus depth vectors $\boldsymbol{P}$, $\boldsymbol{Q}$, and $\boldsymbol{T}$, from Eq. (7), the fitted strain invariants $\hat{\boldsymbol{p}}$, $\hat{\boldsymbol{q}}$, and $\hat{\boldsymbol{t}}$ are determined from

$$\hat{\boldsymbol{p}} = \frac{1+\nu}{E} \bar{\boldsymbol{a}} \boldsymbol{P}, \tag{9}$$

$$\hat{\boldsymbol{q}} = \frac{1}{E}\bar{\mathbf{b}}\boldsymbol{Q},$$

$$\hat{\boldsymbol{t}} = \frac{1}{E}\bar{\mathbf{b}}\boldsymbol{T}.$$

The fitted and measured strain invariants are nearly equal, $\hat{\boldsymbol{p}} \approx \boldsymbol{p}$, $\hat{\boldsymbol{q}} \approx \boldsymbol{q}$, and $\hat{\boldsymbol{t}} \approx \boldsymbol{t}$ when the value of α is highly negative (β near zero) but for a typical value of α there is a finite strain misfit defined as

$$\begin{aligned} \boldsymbol{p}_{\text{misfit}} &= \boldsymbol{p} - \hat{\boldsymbol{p}}, \\ \boldsymbol{q}_{\text{misfit}} &= \boldsymbol{q} - \hat{\boldsymbol{q}}, \\ \boldsymbol{t}_{\text{misfit}} &= \boldsymbol{t} - \hat{\boldsymbol{t}}. \end{aligned} \tag{10}$$

The value of the regularization parameters α, and subsequently β in Eq. (4), significantly influence the calculated residual stress. In an extreme case with no regularization ($\alpha << 0$, so $\beta \approx 0$), the measured strains are fit exactly and strain measurement noise is amplified in the calculated residual stress. In the other extreme case, with $\alpha \approx 0$, the measured strains will be overly smoothed and the calculated residual stress versus depth profile will likely miss important features. A specific value of α must be selected during data reduction, and since the best value is not known *a priori* the selection increases uncertainty in the measured residual stress.

2.3. Uncertainty estimation

Two stress uncertainty sources will be used to determine the total uncertainty in the hole-drilling measurements. The first uncertainty source is the strain uncertainty ($\mathbf{U}_{\sigma,\varepsilon}$) that determines the uncertainty in the calculated stress due to uncertainty in strain. This was established by Prime and Hill [15] and is given by:

$$\begin{aligned} \mathbf{U}^2_{\boldsymbol{\sigma_P},\boldsymbol{\varepsilon}_\mathbf{p}} &= diag\left(\boldsymbol{V_P}\left[DIAG\left(\boldsymbol{U}^{\boldsymbol{2}}_{\boldsymbol{\varepsilon}_p}\right)\right]\boldsymbol{V}^{\boldsymbol{T}}_{\boldsymbol{P}}\right), \\ \mathbf{U}^2_{\boldsymbol{\sigma_Q},\boldsymbol{\varepsilon_q}} &= diag\left(\boldsymbol{V_Q}\left[DIAG\left(\boldsymbol{U}^{\boldsymbol{2}}_{\boldsymbol{\varepsilon}_q}\right)\right]\boldsymbol{V}^{\boldsymbol{T}}_{\boldsymbol{Q}}\right), \end{aligned} \tag{11}$$

$$\mathbf{U}^2_{\boldsymbol{\sigma_T},\boldsymbol{\varepsilon_t}} = diag\left(\boldsymbol{V_T}\left[DIAG\left(\boldsymbol{U}^{\boldsymbol{2}}_{\boldsymbol{\varepsilon_t}}\right)\right]\boldsymbol{V}^{\boldsymbol{T}}_{\boldsymbol{T}}\right)$$

where $\mathbf{U}^2_{\boldsymbol{\sigma_P},\boldsymbol{\varepsilon_p}}$, $\mathbf{U}^2_{\boldsymbol{\sigma_Q},\boldsymbol{\varepsilon_q}}$, $\mathbf{U}^2_{\boldsymbol{\sigma_T},\boldsymbol{\varepsilon_t}}$ are vectors of the squares of stress uncertainties caused by uncertainties in the measured strain invariants at each cut depth, *diag* is an operator that provides a vector of the diagonal elements of a square matrix, DIAG is an operator that provides a diagonal matrix from a vector, $\boldsymbol{V}$ is defined in Eq. (8), and vectors of strain invariant uncertainties are

$$\begin{aligned} \boldsymbol{U}_{\varepsilon_p} &= max(\boldsymbol{p}_{\text{misfit}}, e), \\ \boldsymbol{U}_{\varepsilon_q} &= max(\boldsymbol{q}_{\text{misfit}}, e), \\ \boldsymbol{U}_{\varepsilon_t} &= max(\boldsymbol{t}_{\text{misfit}}, e), \end{aligned} \tag{12}$$

where e is a lower limit of strain uncertainty taken as the precision inherent to the experimental apparatus and for this work was taken as 0.25 με (based on the precision of the strain reader used in the following measurements).

The second uncertainty source to be addressed is the uncertainty arising from the choice of the regularization parameters in Eq. (4), which will be called the regularization uncertainty. This uncertainty arises because the choice of α (and subsequently β) in Eq. (4) can significantly influence the calculated residual stress and optimal regularization is unknown and uncertain.

The uncertainty estimation scheme employed here follows the approach recently developed for slitting [16] and consists of taking the standard deviation of the calculated residual stress over a selected range of α (α_P, α_Q, α_T) values. For a specific value of $\alpha = \hat{\alpha}$, the regularization uncertainty is established by assessing a set of residual stress invariant versus depth results computed using different values of α near $\hat{\alpha}$ (i.e., different amounts of regularization), which defines the sensitivity of the computed residual stress to α. Each member of the set of residual stress results is computed for a range of α called α_{subset}.

The range α_{subset} is defined by two key characteristics, the number of values that it contains, M, and the range of α that it spans. The present work uses a logarithmically spaced set of $M = 60$ values of α spanning a range $\alpha_{subset} = [\hat{\alpha} \pm R]$ where $R = 2$. The justification for the value of the R parameter is presented later. The value for the M parameter was previously established in [16]. Vectors of regularization uncertainty versus depth, $\boldsymbol{U}_{\sigma_P,\mathrm{reg}}$, $\boldsymbol{U}_{\sigma_Q,\mathrm{reg}}$, and $\boldsymbol{U}_{\sigma_T,\mathrm{reg}}$ are then defined as the standard deviation of the set of residual stress invariant values at each depth computed for the different values of α in α_{subset}

$$\begin{aligned}
\boldsymbol{U}_{\sigma_P,\mathrm{reg}}(\hat{\alpha}) &= \sqrt{\frac{1}{M-1}\sum_{i=1}^{M}[\boldsymbol{P}_i - \overline{\boldsymbol{P}}]^2}, \\
\boldsymbol{U}_{\sigma_Q,\mathrm{reg}}(\hat{\alpha}) &= \sqrt{\frac{1}{M-1}\sum_{i=1}^{M}[\boldsymbol{Q}_i - \overline{\boldsymbol{Q}}]^2}, \\
\boldsymbol{U}_{\sigma_T,\mathrm{reg}}(\hat{\alpha}) &= \sqrt{\frac{1}{M-1}\sum_{i=1}^{M}[\boldsymbol{T}_i - \overline{\boldsymbol{T}}]^2}
\end{aligned} \tag{13}$$

where the vectors $\boldsymbol{P}_i$, $\boldsymbol{Q}_i$, and $\boldsymbol{T}_i$ reflect stresses computed for values of α in α_{subset} and $\overline{\boldsymbol{P}}$, $\overline{\boldsymbol{Q}}$, and $\overline{\boldsymbol{T}}$ are the average values of the stress invariants at the set of depths.

The total uncertainty is taken as the root of the sum of squares (RSS) of the two uncertainty sources

$$\begin{aligned}
\boldsymbol{U}^2_{\sigma_P,\mathrm{tot}} &= \boldsymbol{U}^2_{\sigma_P,\varepsilon_p} + \boldsymbol{U}^2_{\sigma_P,\mathrm{reg}}, \\
\boldsymbol{U}^2_{\sigma_Q,\mathrm{tot}} &= \boldsymbol{U}^2_{\sigma_Q,\varepsilon_q} + \boldsymbol{U}^2_{\sigma_Q,\mathrm{reg}}, \\
\boldsymbol{U}^2_{\sigma_T,\mathrm{tot}} &= \boldsymbol{U}^2_{\sigma_T,\varepsilon_t} + \boldsymbol{U}^2_{\sigma_T,\mathrm{reg}}.
\end{aligned} \tag{14}$$

The stresses are computed using the stress invariants as

$$\boldsymbol{\sigma}_{xx} = \boldsymbol{P} - \boldsymbol{Q},$$
$$\boldsymbol{\sigma}_{yy} = \boldsymbol{P} + \boldsymbol{Q},$$
$$\boldsymbol{\tau}_{xy} = \boldsymbol{T}. \tag{15}$$

The stress uncertainties are computed using the stress invariant uncertainties as

$$\boldsymbol{U}^2_{\sigma_{xx},\mathrm{tot}} = \boldsymbol{U}^2_{\sigma_{yy},\mathrm{tot}} = \boldsymbol{U}^2_{\sigma_P,\mathrm{tot}} + \boldsymbol{U}^2_{\sigma_Q,\mathrm{tot}},$$
$$\boldsymbol{U}^2_{\tau_{xy},\mathrm{tot}} = \boldsymbol{U}^2_{\sigma_T,\mathrm{tot}}. \tag{16}$$

Additionally, the strain and regularization uncertainty in the stresses are computed using the stress invariant uncertainties as

$$\boldsymbol{U}^2_{\sigma_{xx},\mathrm{reg}} = \boldsymbol{U}^2_{\sigma_{yy},\mathrm{reg}} = \boldsymbol{U}^2_{\sigma_P,\mathrm{reg}} + \boldsymbol{U}^2_{\sigma_Q,\mathrm{reg}},$$
$$\boldsymbol{U}^2_{\tau_{xy},\mathrm{reg}} = \boldsymbol{U}^2_{\sigma_T,\mathrm{reg}} \tag{17}$$

and

$$\boldsymbol{U}^2_{\sigma_{xx},\varepsilon} = \boldsymbol{U}^2_{\sigma_{yy},\varepsilon} = \boldsymbol{U}^2_{\sigma_P,\varepsilon} + \boldsymbol{U}^2_{\sigma_Q,\varepsilon},$$
$$\boldsymbol{U}^2_{\tau_{xy},\varepsilon} = \boldsymbol{U}^2_{\sigma_T,\varepsilon} \tag{18}$$

2.4. Regularization parameter

The selection of α (and therefore β) can be determined using the recommendation in ASTM E837-13 [8]. In ASTM E837-13, the regularization is chosen such that the "standard errors" in the strain invariants (p_{std}, q_{std}, t_{std}) are within 5% of the root mean squares of the misfit vectors (p_{rms}, q_{rms}, t_{rms}). The "standard errors" in the strain invariants are determined from the measured strain invariant data using

$$p_{std}^2 = \sum_{j=1}^{N-3} \frac{\left(p_j - 3p_{j+1} + 3p_{j+2} - p_{j+3}\right)^2}{20(N-3)} \tag{19}$$

$$q_{std}^2 = \sum_{j=1}^{N-3} \frac{\left(q_j - 3q_{j+1} + 3q_{j+2} - q_{j+3}\right)^2}{20(N-3)},$$

$$t_{std}^2 = \sum_{j=1}^{N-3} \frac{\left(t_j - 3t_{j+1} + 3t_{j+2} - t_{j+3}\right)^2}{20(N-3)}.$$

and the mean squares of the misfit vectors are defined as

$$p_{rms}^2 = \frac{1}{N}\sum_{j=1}^{N} (p_{\text{misfit}})_j^2, \tag{20}$$

$$q_{rms}^2 = \frac{1}{N}\sum_{j=1}^{N} (q_{\text{misfit}})_j^2,$$

$$t_{rms}^2 = \frac{1}{N}\sum_{j=1}^{N} (t_{\text{misfit}})_j^2.$$

It is possible for this selection strategy to prescribe overly large α values (α_P, α_Q, α_T) and produce overly smooth stress data. A modified approach using the strain invariant misfits was explored here. We call this approach the *misfit plateau* approach and refer to the recommendation in ASTM E837-13 as the ASTM approach. The misfit plateau approach will select α values (α_P, α_Q, α_T) as the minimum α values that are selected from either the ASTM approach or at α values where the RMS strain invariant misfit is at a value of 95% of where the of the RMS strain invariant misfits reach a steady value (i.e., a plateau).

2.5. Regularization parameter selection procedure

The regularization parameters in this work were selected using the following procedure. First, apply the above formulae (Eq. (1) through (10)) to calculate stress and strain misfits invariants over a range of α values, starting with a highly negative α value (-20) that increases in small increments (~0.1) to an arbitrary maximum α value where the maximum misfit invariant exceeds a set maximum value (10 με).

Next, calculate the "standard errors" (p_{std}, q_{std}, t_{std}) and root mean squares of the strain invariant misfit vectors (p_{rms}, q_{rms}, t_{rms}) as given in Eq. (19) and (20). Next determine the lowest α values where p_{rms}, q_{rms}, t_{rms} are within 5% of p_{std}, q_{std}, t_{std}. This gives $\alpha_{P,\,ASTM}$, $\alpha_{Q,\,ASTM}$, and $\alpha_{T,\,ASTM}$.

Using the RMS strain invariant misfits (p_{rms}, q_{rms}, t_{rms}), determine the value where each plateaus. To determine this value, assume the plateaued value is where p_{rms}, q_{rms}, t_{rms} are changing less than 1% for a 0.1 change of α (applied separately for p_{rms}, q_{rms}, t_{rms}). Typically, p_{rms}, q_{rms}, t_{rms} plateaus occur for large values of α and is then nominally constant over a wide range of increasing α values (see Fig. 12 for an example). Next, find the α values where (p_{rms}, q_{rms}, t_{rms}) = 0.95($p_{rms,\,plateau}$, $q_{rms,\,plateau}$, $t_{rms,\,plateau}$) and this will provide $\alpha_{P,\,plateau}$, $\alpha_{Q,\,plateau}$, and $\alpha_{T,\,plateau}$.

Lastly compare the $\alpha_{P,\,ASTM}$, $\alpha_{Q,\,ASTM}$, and $\alpha_{T,\,ASTM}$ with $\alpha_{P,\,plateau}$, $\alpha_{Q,\,plateau}$, and $\alpha_{T,\,plateau}$. If $\alpha_{plateau} + 0.5 < \alpha_{ASTM}$, then use $\alpha_{plateau}$ otherwise use α_{ASTM}. This criterion is used to ensure the plateau approach is only used when the ASTM approach has significantly oversmoothed the data.

2.6. Numerical experiment to evaluate the uncertainty estimation scheme

To determine whether the regularization uncertainty as defined above provides a useful estimate of regularization error, a numerical experiment is performed. The numerical experiment consists of choosing a stress distribution (initialized residual stress) and determining the strains that would occur after each of a set of cut depth increments (initialized strain). The initialized stress is a smoothly varying stress profile similar to the stress profile from machining [17,18] and is defined using a polynomial function

$$\begin{aligned} \sigma_x(z) = \sigma_y(z) &= 100\cdot(1/21 - (1-z)^{20}) \text{ for } 0 < z \leq 1 \text{ mm} \\ \tau_{xy}(z) &= 0 \end{aligned} \tag{21}$$

as shown in Fig. 2a. The numerical experiment used cut depths specified in ASTM E837 where $N = 20$ and $h_i = 0.05, 0.10, \ldots, 1.0$ mm.

The strains due to stresses in Eq. (21) are directly determined using the $\bar{\mathbf{a}}$ and $\bar{\mathbf{b}}$ calibration coefficient matrices in ASTM E837. This is accomplished by using the constitutive equation relating stress to strain (Eq. (1) through (3)) so that

$$\boldsymbol{\varepsilon}_{0^\circ} = \frac{(1+\nu)\bar{\mathbf{a}}\boldsymbol{P} - \bar{\mathbf{b}}\boldsymbol{Q}}{E}$$

$$\boldsymbol{\varepsilon}_{90^\circ} = \frac{(1+\nu)\bar{\mathbf{a}}\boldsymbol{P} + \bar{\mathbf{b}}\boldsymbol{Q}}{E} \tag{22}$$

$$\boldsymbol{\varepsilon}_{225^\circ} = \frac{2(1+\nu)\bar{\mathbf{a}}\boldsymbol{P} - \bar{\mathbf{b}}\boldsymbol{T}}{E}$$

where $\boldsymbol{P}$, $\boldsymbol{Q}$, and $\boldsymbol{T}$ are calculated from Eq. (3) and Eq. (21), at depths corresponding to the average of the neighboring depth increments [8].

The resulting strains are shown in Fig. 2b. After the strains are determined, noise is added to the strains. The added noise is normally distributed with a standard deviation of 0.5 με and when added to the initialized strains provides the noisy strains of Fig. 2b. The magnitude of the added noise was approximated from the precision of a range of commercially available strain readers. Residual stress and uncertainties are subsequently determined from the noisy strains for a range of α values. Since both the non-noisy strains and the noisy strains are known, the error arising from the strain noise can be determined and provides a useful benchmark to assess the uncertainty estimation scheme.

2.7. Acceptance criterion

To test whether the uncertainty estimate accurately estimates the random uncertainty that is present during a hole-drilling measurement, an acceptance criterion will be used. The acceptance criterion will determine the *acceptance fraction* which is the percentage of points where the calculated stress ± its estimated uncertainty contains the true value, as was done in earlier work [16,19,20]. For the numerical experiment, the true stress profile is known (the initialized residual stress). For the repeatability studies,

the true value is taken as the mean of the repeated measurements because that is the best available estimate of the underlying residual stress field (and the difference between the mean and each measurement provides an approximation of the random measurement error, assuming each specimen has a similar initial residual stress state). If the underlying stress measurement uncertainty follows a normal distribution, a useful uncertainty estimate would provide an acceptance fraction of 68%.

2.8. Repeatability experiments

Both specimens used for repeatability experiments have nominally identical geometry and are fabricated from low stress rolled plate. The plate dimensions have a nominal length of 381 mm (15 in), width of 190.5 mm (7.5 in), and thickness of 25.4 mm (1 in), as can be seen in Fig. 1. The coordinate system used here has the x-direction along the width, the y-direction along the length, and the z-direction into the thickness (Fig. 1). The aluminum specimen is made from a 7050-T7451 aluminum plate that had been stress relieved by stretching and the titanium specimen is made from Ti-6Al-4V titanium alloy that had been mill annealed and stress relieved. Both specimens underwent shot peening to introduce significant magnitude residual stresses that are nominally equibiaxial. The aluminum plate is assumed to have an elastic modulus of 71.7 GPa (10,400 ksi) and a Poisson's ratio of 0.33. The titanium plate is assumed to have an elastic modulus of 113.8 GPa (16,500 ksi) and a Poisson's ratio of 0.34.

For each specimen, hole-drilling repeatability is assessed by performing 12 hole-drilling measurements on each specimen. The measurements are made at identical locations in each specimen, at selected points on a grid with 25.4 mm (1 in) spacing in the x and y-directions. The selected points are more than 50 mm from the free edges of the specimen. The 25.4 mm spacing ensures that the measurements don't affect one another [21]. The hole is drilled using an automated, hands-free, bespoke milling machine, with a 1.59 mm diameter end mill cutter, and a drill speed of 80,000 rpm. Strains are

measured using an ASTM Type A strain gage rosette with gage lengths of 1.59 mm (0.062 in) (Vishay CEA-13-062UL-120) and a 5.13 mm (0.202 in) diameter gage circle. The drilled holes have a diameter of 2 mm (0.080 in) and hole depths are cut from 0.05 mm to 1.00 mm in increments of 0.05 mm (0.002 in to 0.040 in with 0.002 in increments).

Each measurement provides the in-plane stresses (σ_{xx}, σ_{yy}, τ_{xy}) as a function of depth from the surface. All measurements are performed in a consistent manner to assess measurement repeatability. Given data from the hole-drilling measurements, the mean and repeatability standard deviation are calculated as functions of depth using standard formulae for the two repeatability experiments.

3. RESULTS

3.1. Numerical experiment

The initialized stresses and the calculated stresses with added noise and without regularization are shown in Fig. 3. The initialized normal stresses follow Eq. (21) with a minimum value of -100 MPa at $z = 0$. The stresses calculated without regularization follow the initialized stresses very well at shallow depths, but at larger depths have sharp gradients and differ from the initialized stresses by up to 60 MPa (55% of the stress range).

The misfit versus cut depth for various levels of regularization is shown in Fig. 4. For very low regularization there is essentially no misfit (i.e., the data are fit perfectly), but the noise in the data have a significant effect on the calculated stress (Fig. 3). The misfit for the selected regularization approximates the noise that was introduced to the strain data. When a high amount of regularization is used, misfits are very high (up to 6 με, Fig. 4).

One component of calculated stress (σ_{xx}) is shown in Fig. 5a for the chosen α values. The calculated stress matches the initialized stress well. Fig. 5b compares the absolute value of the stress error (calculated – initialized) to the total uncertainty and the uncertainties due to strain misfit and

regularization. The total uncertainty is in reasonable agreement with the error, with both having high values at small depth, lower values at moderate depth, and larger values near the final cut depths. The maximum uncertainty is higher than the maximum error (13.5 MPa error vs. 6.0 MPa total uncertainty). Both the regularization and strain uncertainties are significant contributors to the total uncertainty (Fig. 5b). The acceptance criterion (i.e., the calculated stress ± the total uncertainty contains the initialized stress) is met at 70.0% of points for the case shown in Fig. 5 (σ_{xx}) and of an average of 77.5% of points for σ_{xx} over 50 iterations with independent, noisy data added to the initialized strains (for other stress components the acceptance criterion was at was 78.3% for σ_{yy} and 79.9% for τ_{xy} over the 50 iterations).

3.2. Repeatability study: Shot peened aluminum plate

The results of the repeatability study using the shot peened aluminum plate can be seen in Fig. 6. The results show that all 12 measurements (Fig. 6a,c,e) are in nominal agreement and show an equibiaxial stress state with low magnitude shear stress. Both σ_{xx} and σ_{yy} (Fig. 6a,c) show a high magnitude compressive stress at the surface (min ≈ -275 MPa) that quickly decays to low magnitude compressive stress (falls to -30 MPa at a depth of 0.3 mm). The shear stress (Fig. 6e) is low over the entire cut depth, but has somewhat larger magnitude near the surface (max ≈ 25 MPa).

The repeatability standard deviation of the population and the estimated uncertainty for each measurement are shown in Fig. 6b,d,f. There is general agreement over the entire cut depth between the repeatability standard deviation and the estimated uncertainty. The uncertainty in both σ_{xx} and σ_{yy} show similar trends with the uncertainty being largest near the surface (max ≈ 25 MPa), falling below 5 MPa for depth greater than about 0.5 mm, and then increasing to ~12 MPa near the final depth. The repeatability standard deviation follows the same trend, but with smaller peaks (~15 MPa) near the surface, falling below 5 MPa for depth greater than about 0.25 mm, and 7 MPa at the final depth. The shear stress uncertainty is very small (most values are below 3 MPa) and the shear stress repeatability

standard deviation is somewhat larger at shallow depth (~12 MPa), but falls below 4 MPa for depth larger than 0.2 mm.

The acceptance fraction for each measurement is shown in Fig. 7. The mean acceptance fractions for the stress components are 75.4%, 76.7%, and 36.3% for σ_{xx}, σ_{yy}, and τ_{xy}, respectively. Some measurements meet the acceptance criteria at fewer points than expected for some stress components. The shear stress component falls far below the expected acceptance fraction, indicating that the uncertainty estimator for shear stress is too small.

3.3. Repeatability study: Shot peened titanium plate

The results of the repeatability study using the shot peened titanium plate can be seen in Fig. 8. The results show that all 12 measurements (Fig. 8a,c,e) are in nominal agreement and show an equibiaxial stress state with low magnitude shear stress. Both σ_{xx} and σ_{yy} (Fig. 8a,c) show very high magnitude compressive stress at the surface (min ≈ -800 MPa) that quickly decays to low magnitude stress (falls to ±10 MPa at a depth of 0.2 mm). The shear stress (Fig. 8e) is low in magnitude (under ±50 MPa) over the entire cut depth, but has more variability near the surface (depth < 0.2 mm).

The repeatability standard deviation and uncertainty for each measurement are shown in (Fig. 8b,d,f) and are in general agreement. The uncertainty in σ_{xx} and σ_{yy} show similar trends, with the uncertainty being largest at the surface (max ≈ 95 MPa), falling to ~8 MPa beyond 0.3 mm, and finally increasing to ~20 MPa at depth of 1 mm. The repeatability standard deviation follows the same trend as the uncertainties, but with smaller peaks (~60 MPa at the surface and 5 MPa at the final cut depth). The shear stress uncertainty is significantly smaller than the normal stress uncertainty and is also largest near the surface (max ≈ 25 MPa) and small (less than 8 MPa) beyond 0.25 mm. The shear stress repeatability standard deviation is initially larger than the uncertainty, especially at the surface (~51 MPa vs. ~20 MPa) and is similar to the uncertainties beyond 0.3 mm.

The acceptance fraction for each measurement is shown in Fig. 9. The mean acceptance fractions are 78.3%, 86.7%, and 33.3% for σ_{xx}, σ_{yy}, and τ_{xy}, respectively. The acceptance fractions follow the same trends as the acceptance fractions for the aluminum plate, namely some measurements meet the acceptance criteria at fewer points than expected and the acceptance fraction for shear stress falls far below the expected value.

4. DISCUSSION

4.1. Numerical experiment

The calculated stresses for the numerical experiment (Fig. 3) show the need for regularization in the stress calculation procedure, since without it, the calculated stresses have significant, erroneous gradients (55% of the stress range), especially at deeper depths. The numerical experiment also shows the total uncertainty estimate (Fig. 5) to be a reasonable predictor of the error present in the case investigated.

To further illustrate how the uncertainty estimate performs, the RMS uncertainties (regularization, strain, and total) and the RMS error for σ_{xx} are shown in Fig. 10 over a range of α values (-20 to 6.7). The results show that the total uncertainty is representative of the error for a relatively narrow band of α values (-12 to -8) and that it significantly underestimates the error for low and high α values. This highlights the importance of choosing a reasonable α value to simultaneously minimize error, produce an accurate uncertainty estimate, and accurately calculate stress.

The numerical experiment was useful in determining the α scaling factor, R, used in the regularization uncertainty estimate. The numerical experiment was run with numerous values of R, ranging from 0 to 5. For each R, the numerical experiment was run with 50 sets of independent, random noise added to the strain data (same set of strain data for each R iteration). The mean acceptance fraction over the range of R values is shown in Fig. 11a using three different α selection criteria. One α selection

criterion was the ASTM selection criterion (described above), another was where α was selected at 95% of the RMS misfit plateau (described above), and the final α selection criterion choose an α where the RMS misfit equals the RMS of the applied noise (that value should result in an optimally smoothed stress where the noise is essentially removed from the calculated stress). The results show the same trends for all α selection criteria, with the mean acceptance fraction initially low (30% for $R = 0$) and gradually increasing to ~90%. R was set to 2 to produce a mean acceptance fraction that was somewhat larger than necessary (78-80% vs. 68%). The mean acceptance fraction versus α is shown in Fig. 11b for $R = 2$ (using the misfit plateau selection criterion) to further illustrate the effect of the choice of α on the mean acceptance fraction. The results show the mean acceptance fraction for low α values is smaller than the expected value of 68%, peaks for moderate α values, then quickly decays to very low values (between 0 and ~15%). This shows that as the data are oversmoothed, the calculated stress isn't accurately reflecting the underlying data.

Two additional numerical experiments were performed (not shown for brevity). One used a constant stress of 100 MPa and the other used a linearly varying stress profile that started at 100 MPa at the surface and decreased to 0 at a depth of 1 mm. For both cases, when the ASTM α selection criterion was used, the selected α was very large and caused there to be large errors in the calculated stress. To remedy the poor selection of α in these cases, the α selection criterion was modified (as described earlier). The additional step consisted of determining the α value where the RMS strain invariant misfit reaches 95% of the value where it plateaus (shown in Fig. 12 for the original numerical experiment). This α value is a reasonable approximation of the ideal α value because, if the RMS invariant misfits are no longer increasing, the stress profile is smoothed to an acceptable degree. For the linear stress profile case, the ASTM selected α value was 5.0 and the plateau approach α value was -3.1, so the difference is significant. However, this issue only appeared during the two numerical experiments where the stresses where straight lines, so perhaps this is an issue that will rarely present itself in practical experiments.

The α selected using the ASTM α selection criteria worked well for all the measurements in the repeatability experiments reported here, so the plateau criterion is required in only certain cases.

4.2. Repeatability experiments

Results for both repeatability experiments follow the trends from the numerical experiment, with repeatability standard deviation being largest at the surface, falling to a significantly smaller value for most of the remaining cut depth, and then increasing at the final depths. The repeatability standard deviations at the surface, over most of the cut depth, and near the final cut depth are about 25, 5, and 12 MPa for the shot peened aluminum plate and about 60, 6, and 5 MPa for the shot peened titanium plate. Additionally, the mean acceptance fraction was around the expected value of 68% in both repeatability studies for normal stresses, but about 50% of the expected value for shear stress. The numerical character of the compliance for the initial cut depths contributes to the larger uncertainty at shallow depths and additional uncertainty may arise from errors in establishing the zero-depth datum.

The present repeatability standard deviations are nominally consistent with those reported in earlier work [8,9], although the earlier studies are difficult to directly compare to the work here. Of the four specimens assessed in the earlier studies, only one had a material in common with the present study, the friction stir welded aluminum specimens of [9]. That study found larger peak repeatability standard deviation than for the shot peened aluminum specimen here (~40 MPa vs. ~15 MPa). The other specimens had standard deviations that are similar to the values found here, but only a qualitative comparison can be made. For reference, the repeatability standard deviations reported in [8] are 14 MPa for stress relieved AISI 1018 specimens and 12 MPa for stress relieved 304 stainless steel specimens. Interlaboratory reproducibility standard deviations in [9] were estimated to be around 40 MPa for friction stir welded aluminum specimens and several hundred MPa for shot peened steel specimens. Several additional caveats in the previous studies are notable, such as in [8] where the stresses were

assumed to be uniform with depth (which would cause the repeatability standard deviations to be lower than those for a non-uniform case [8]) and in [9] where the study reported interlaboratory reproducibility rather than intralaboratory repeatability. Additionally, the use of different materials can cause differences in repeatability, where higher elastic modulus leads to larger repeatability standard deviations [22]. The measurements here, and in some of the previous studies, used specimens that had residual stresses induced from shot peening, which causes an equibiaxial stress state. Such a stress state would reduce effects of the $\bar{\mathbf{b}}$ calibration coefficient matrices in the stress calculation procedure and thus could reduce the repeatability standard deviation.

Often a series of nominally identical repeated measurements are performed to provide a first order uncertainty assessment rather than relying on a single measurement uncertainty estimator. During repeated measurements, the experimenter would seek to minimize controllable sources of uncertainty. One such source of uncertainty is the selection of α values. As shown above the choice of a α values can have a significant impact on the calculated stress and when the experiment is attempting to minimize uncertainty (using a first order estimate) there is temptation to choose larger α values, such that the stress will be smoother and more consistent between measurements. This will minimize the repeatability standard deviation (and first order uncertainty estimate), but often at the expense of measurement accuracy. To illustrate this point, the RMS repeatability standard deviation for σ_{xx} is shown in Fig. 13 (dashed red line in) in the shot peened aluminum plate. This shows the repeatability standard deviation monotonically decreases with increasing α, even though the calculated stress is over smoothed as α becomes large. This result shows that even though the precision increases as α increases, as quantified by the repeatability standard deviation, at some point the accuracy decreases with increasing α (and the calculated stress is erroneous). This further raises the issue that α selection is critical and that both the precision and accuracy of a measurement technique need to be considered when such information is available.

4.3. Comparison between hole-drilling machines

As a validation exercise in the development of the bespoke automated milling machine used here, replicate repeatability studies were performed on the same plates using a commercially available manual hole-drilling machine (RS-200, Micro-Measurements). The results from both machines are shown in Fig. 14 for the aluminum plate and in Fig. 15 for the titanium plate. The results show that measurements from each machine are generally self-consistent. The results also show similar stress profiles, where the stresses have peak compression at the surface that decay to low magnitude stress subsurface. However, there are significant differences in results of measurements made with each machine. First, results from the commercial machine have lower magnitude compressive stress at the surface. The average surface stresses (σ_{xx} and σ_{yy}) for the aluminum plate are -275 MPa for the bespoke automated machine and -210 MPa for the commercial machine, with analogous values for the titanium plate being -800 MPa and -550 MPa. Second, the near surface stresses decay more sharply in results from the bespoke automated machine compared to the results from the manual machine, with the depth of significant compressive stress differing by about a factor of two. Third, the repeatability standard deviation is significantly smaller for the measurements from the bespoke automated machine in both samples, but particularly in the titanium sample.

The mean acceptance fraction of σ_{xx} for the commercial manual machine is 38.6% for the shot peened aluminum plate and 43.3% for the shot peened titanium plate, which was significantly different from those found from the bespoke automated machine (75.4% and 78.3%, respectively). The significantly lower mean acceptance fraction from the commercial manual machine is due to the larger variation in the measured stress despite both sets of measurements having similar levels of calculated uncertainty (Fig. 14 and Fig. 15).

The significant differences in the measured stresses between the repeatability studies using different milling machines is concerning. The primary cause of discrepancy is expected to be inferior dimensional control for the hole that are present in the manual machine. Possible sources of bias may be inaccurate cut depth [23] and hole eccentricity [24,25], both of which cause errors because they invalidate assumptions inherent in the stress calculation procedure. The differences in stress could also be caused by differences in cutting induced strains that interfere with the strains due to release of residual stress. The air-driven spindle of the manual machine has no control over cut speed, whereas the electronic spindle of the bespoke automated machine has feedback control, which yields more consistent cutting.

The differences in the stresses measured by the two different milling machines further emphasize that the proposed uncertainty estimate provides a measure of precision and does not indicate measurement accuracy. Additionally, the repeatability standard deviations presume the residual stress in the samples are uniform at all measured locations, which implies that the reported repeatability standard deviations arise from measurement imprecision. Some fraction of the differences in measured stress are likely due to stress field variability, so the reported repeatability standard deviation is likely to be conservative (i.e., larger than would be found with a perfectly uniform stress field).

5. SUMMARY/CONCLUSIONS

Repeatability of hole-drilling residual stress measurements using a bespoke automated machine was determined in two configurations: a shot peened aluminum plate and a shot peened titanium plate. Each repeatability assessment included 12 hole-drilling measurements. The results show similar trends between both studies: larger repeatability standard deviations at the surface that decay quickly (over about 0.3 mm). The repeatability standard deviation was significantly smaller in the aluminum plate (max ≈ 15 MPa) than in the titanium plate (max ≈ 60 MPa).

The work here also developed an uncertainty estimate that includes uncertainty arising from regularization of the measured strains. The uncertainty estimate was tested in a numerical experiment, which showed the uncertainty estimate to reasonably predict the error present in the numerical experiment and to meet a statistically based acceptance criterion. Application of the uncertainty estimate in both repeatability studies showed that the uncertainty estimate was consistent with the repeatability standard deviation (precision) and met the statistically based acceptance criterion.

Repeatability of hole-drilling residual stress was also characterized for a commercially available manual hole-drilling machine (RS-200, Micro-Measurements). The comparison between results from two measurement devices show differences in the measured stresses, which indicate that bias errors may be present in one or both sets of measurements, which are not quantified by the uncertainty estimate nor the repeatability standard deviation.

ETHICAL STATEMENT/CONFLICT OF INTEREST

The authors have no conflicts of interest to disclose and did not involve human or animal participants nor was informed consent applicable.

REFERENCES

[1] ASTM Standard E177-10, Practice for Use of the Terms Precision and Bias in ASTM Test Methods, 2010

[2] S. Lestari, "Residual Stress Measurements of Unblasted and Sandblasted Mild Steel Specimens Using X-Ray Diffraction, Strain-Gage Hole Drilling, and Electronic Speckle Pattern Interferometry (ESPI) Hole Drilling Methods," University of New Orleans, 2004.

[3] M. D. Olson, J. S. Robinson, R. C. Wimpory, and M. R. Hill, "Characterisation of residual stresses in heat treated, high strength aluminium alloy extrusions," *Mater. Sci. Technol.*, vol. 32, no. 14, pp. 1427–1438, 2016.

[4] M. E. Fitzpatrick and A. Lodini, Analysis of Residual Stress by Diffraction using Neutron and Synchrotron Radiation. CRC Press, 2003.

[5] M. B. Prime, T. Gnäupel-Herold, J. A. Baumann, R. J. Lederich, D. M. Bowden, and R. J. Sebring, "Residual stress measurements in a thick, dissimilar aluminum alloy friction stir weld," *Acta Mater.*, vol. 54, no. 15, pp. 4013–4021, Sep. 2006.

[6] D. Upshaw, M. Steinzig, and J. Rasty, "Influence of Drilling Parameters on the Accuracy of Hole-drilling Residual Stress Measurements," in *Engineering Applications of Residual Stress*, Volume 8, Springer New York, 2011, pp. 95–109.

[7] M. Steinzig and T. Takahashi, "Residual Stress Measurement Using The Hole Drilling Method And Laser Speckle Interferometry Part IV: Measurement Accuracy," *Exp. Tech.*, vol. 27, no. 6, pp. 59–63, Nov. 2003.

[8] ASTM Standard E837-13, Standard Test Method for Determining Residual Stresses by the Hole-Drilling Strain-Gage Method, 2013, ASTM International, West Conshohocken, PA

[9] Lord JD, Fry AT, Grant PV, A UK Residual Stress Intercomparison Exercise - An Examination of the XRD and Hole Drilling Techniques, NPL Report MATC(A)98, 2002

[10] Micro-Measurements. Milling Guide for Residual Stress Measurements (Document No.: 11304), Vishay Precision Group; 17-May-2011. Available: http://www.vishaypg.com/docs/11304/rs200.pdf

[11] Schajer GS, Whitehead PS. Hole Drilling and Ring Coring. In: Schajer GS, editor. Practical Residual Stress Measurement Methods. West Sussex, UK: John Wiley & Sons, Ltd; 2013. pp. 29–64. doi:10.1002/9781118402832.ch2

[12] G. S. Schajer, "Measurement of Non-Uniform Residual Stresses using the Hole-Drilling Method. Part I - Stress Calculation Proceedures," *J. Eng. Mater. Technol.*, vol. 110, pp. 338–343, 1988.

[13] G. S. Schajer, "Measurement of Non-uniform Residual Stresses Using the Hole-Drilling Method. Part II - Practical Application of the Integral Method," *J. Eng. Mater. Technol.*, vol. 110, pp. 344–349, 1988.

[14] Schajer, G. S., Hole-drilling residual stress profiling with automated smoothing. *Journal of Engineering Materials and Technology, Transactions of the ASME*, *129*(3), 440–445. https://doi.org/10.1115/1.2744416, 2007

[15] M. B. Prime and M. R. Hill, "Uncertainty, Model Error, and Order Selection for Series-Expanded, Residual-Stress Inverse Solutions," J. Eng. Mater. Technol., vol. 128, no. 2, pp. 175–185, Apr. 2006.

[16] M. D. Olson, A. T. DeWald, M. R. Hill. An uncertainty estimator for slitting method residual stress measurements including the influence of regularization. Exp Mech., 2019

[17] Girinon M, Robin V, Jourden E, Vakiorgue F, Rech J, Feulvarch E. A Method to Characterize Residual Stresses Induced by Machining. Proceedings of the ASME 2016 Pressure Vessels and Piping Conference.

[18] Madariaga A, Perez I, Arrazola PJ, Sanchez R, Ruiz JJ, Rubio FJ. Reduction of distortions in large aluminium parts by controlling machining-induced residual stresses. Int J Adv Manuf Technol. 2018; doi:10.1007/s00170-018-1965-2

[19] Olson MD, DeWald AT, Hill MR, Prime MB. Estimation of Uncertainty for Contour Method Residual Stress Measurements. Exp Mech. 2014;55: 577–585.

[20] Olson MD, DeWald AT, Hill MR. Validation of a Contour Method Single-Measurement Uncertainty Estimator. Exp Mech. 2018;58: 767–781. doi:10.1007/s11340-018-0385-4

[21] D. Upshaw, M. Steinzig, and J. Rasty, "Influence of Drilling Parameters on the Accuracy of Hole-Drilling Residual Stress Measurements," in *Engineering Applications of Residual Stress*, Volume 8,2011, pp. 95-109.

[22] Olson MD, DeWald AT, and Hill MR, “Repeatability of Contour Method Residual Stress Measurements for a Range of Materials, Processes, and Geometries,” *Matls. Perf. Charact.*, vol. 7, no. 4, p. 20170044, 2018.

[23] Schajer GS, Altus E. Stress Calculation Error Analysis for Incremental Hole-Drilling Residual Stress Measurements. J Eng Mater Technol. American Society of Mechanical Engineers; 1996;118: 120–126. doi:10.1115/1.2805924

[24]Ajovalasit A. Measurement of residual stresses by the hole-drilling method: Influence of hole eccentricity. J Strain Anal Eng Des. IMECHE; 1979;14: 171–178. doi:10.1243/03093247V144171

[25] Barsanescu P, Carlescu P. Correction of errors introduced by hole eccentricity in residual stress measurement by the hole-drilling strain-gage method. Measurement. Elsevier; 2009;42: 474–477. doi:10.1016/j.measurement.2008.09.002

FIGURES

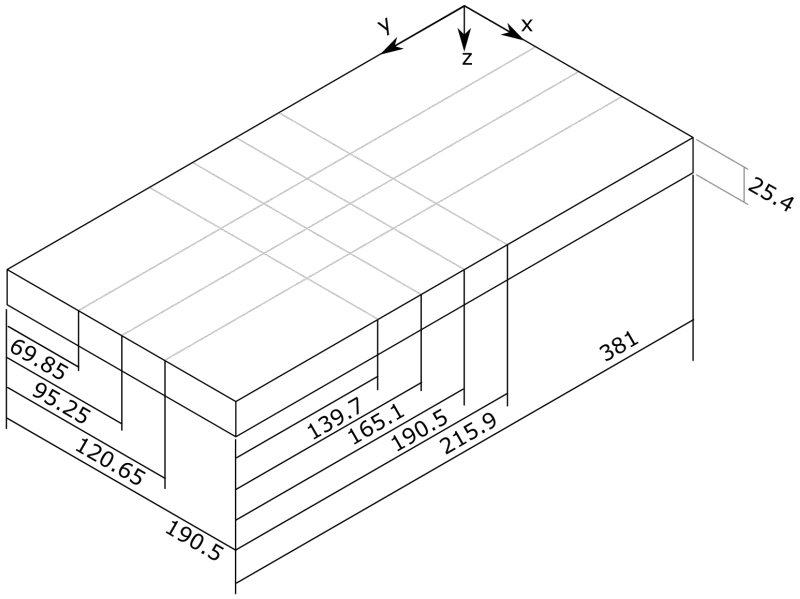

Fig. 1 – Diagram of the aluminum and titanium shot peened plate. The measurement locations are at cross-hatched lines. Dimensions in mm

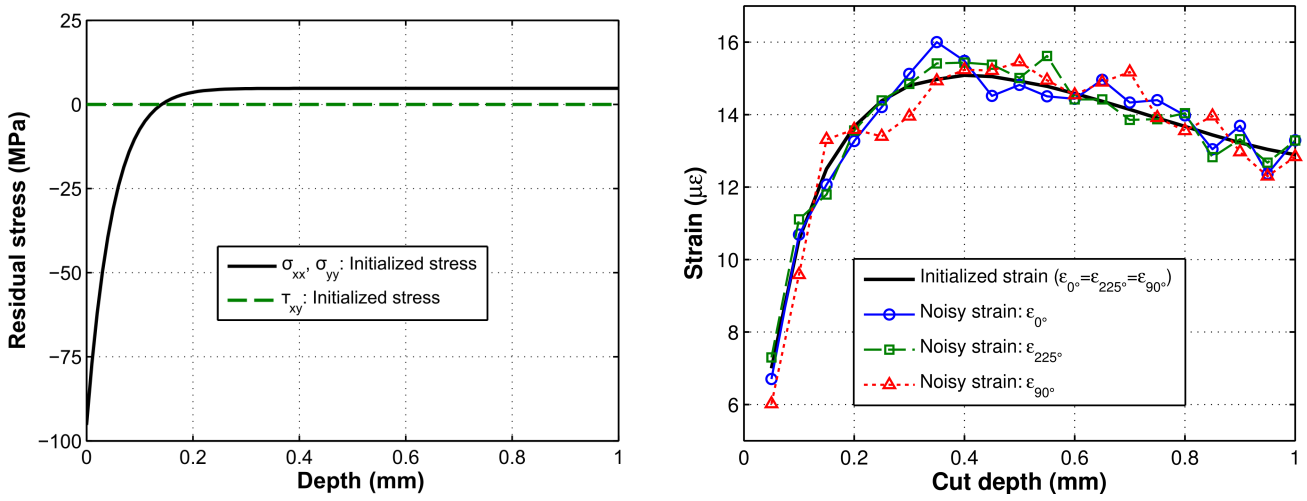

Fig. 2 – Initialized (a) stress and (b) strain for the numerical experiment

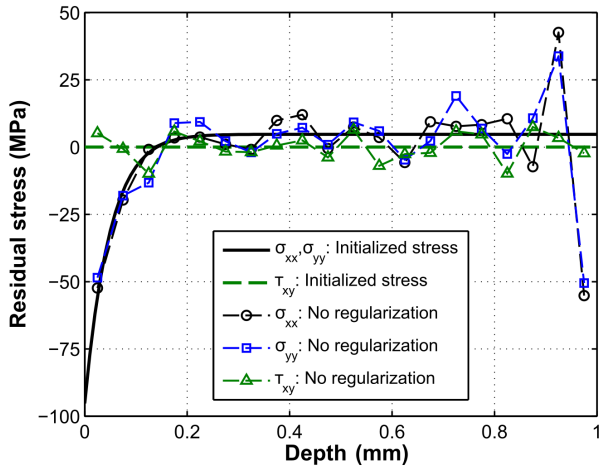

Fig. 3 – Initialized stresses and calculated stresses with added noise and no regularization (i.e., no smoothing) for the numerical experiment

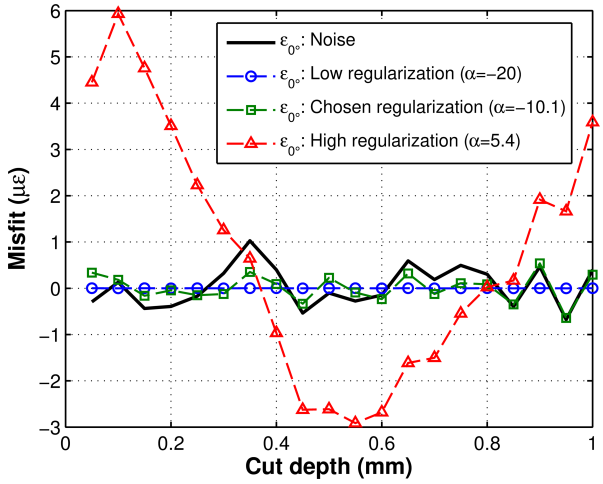

Fig. 4 – Misfit versus cut depth for various levels of regularization for the numerical experiment as well as noise added to the signal

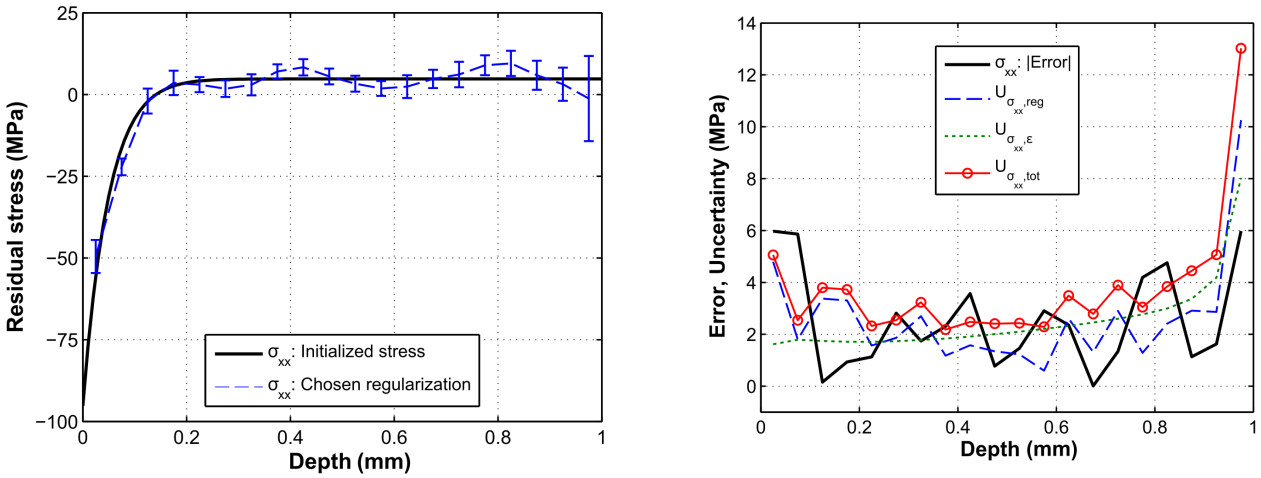

(a) (b)

Fig. 5 –(a) Initialized and calculated stress and (b) uncertainty and error for the numerical experiment (σ_{xx})

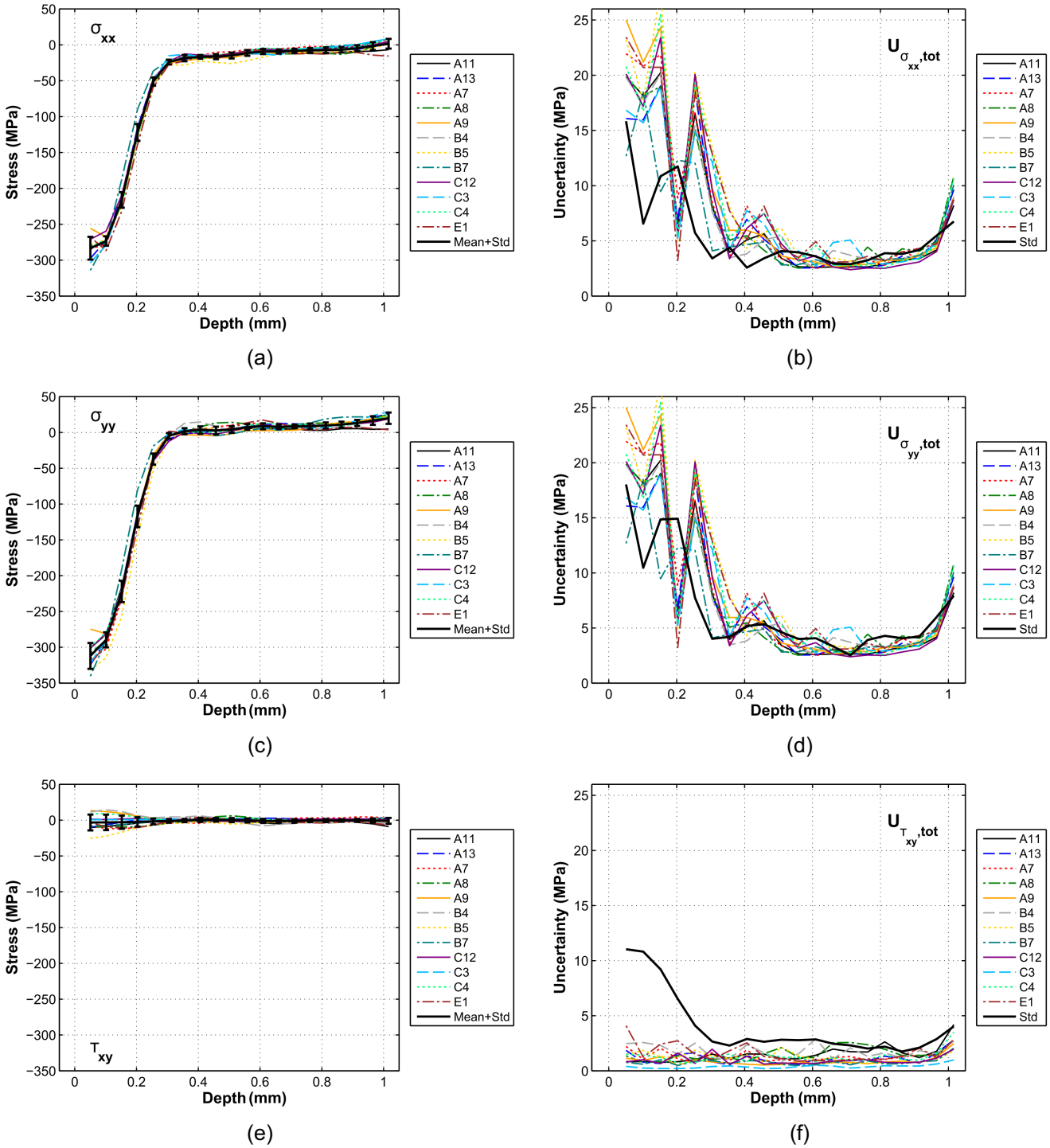

Fig. 6 – Repeatability data for the shot peened aluminum plate stress (and mean with the repeatability standard deviation shown as error bars) (left column) (a) σ_{xx}, (c) σ_{yy}, (e) τ_{xy} and uncertainty and repeatability standard deviation (right column) (b) σ_{xx}, (d) σ_{yy}, (f) τ_{xy}

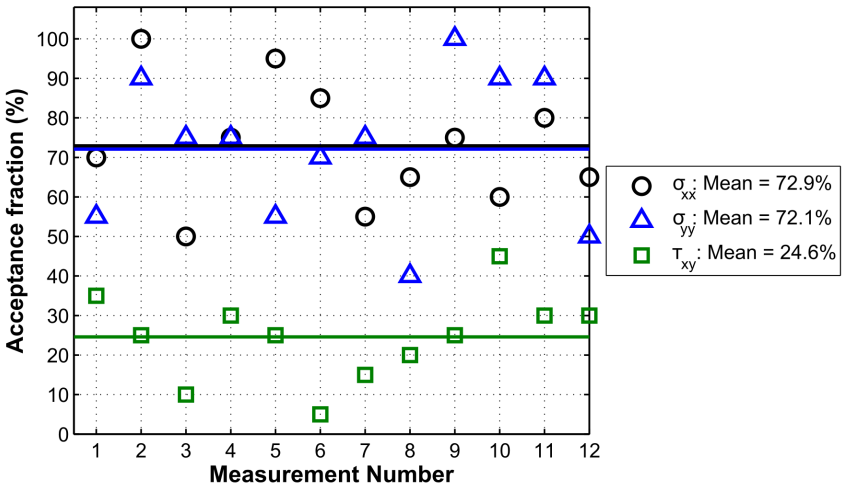

Fig. 7 – Acceptance fraction for each measurement in the shot peened aluminum plate repeatability experiment

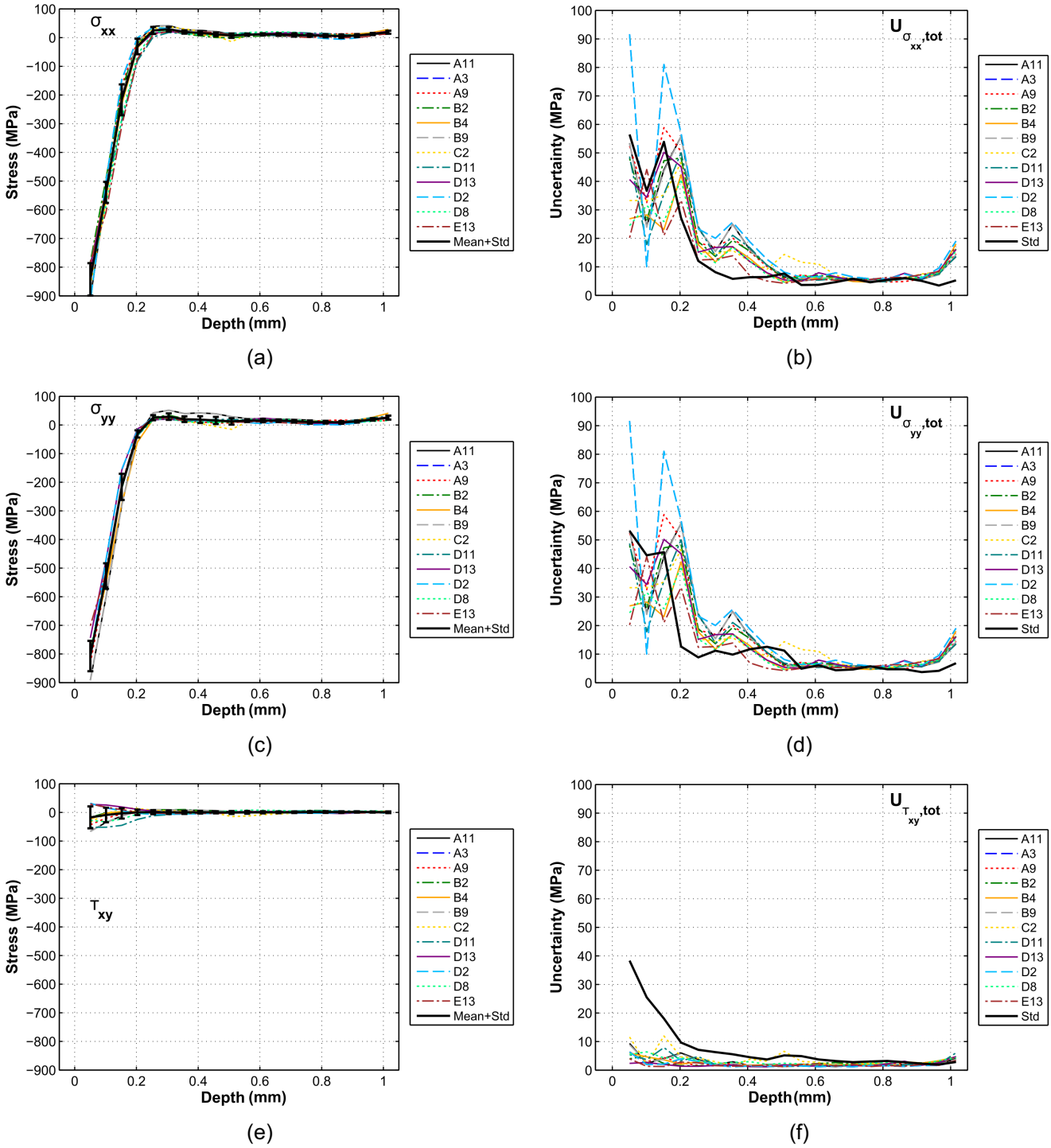

Fig. 8 – Repeatability data for the shot peened titanium plate stress (and mean with the repeatability standard deviation shown as error bars) (left column) (a) σ_{xx}, (c) σ_{yy}, (e) τ_{xy} and uncertainty and repeatability standard deviation (right column) (b) σ_{xx}, (d) σ_{yy}, (f) τ_{xy}

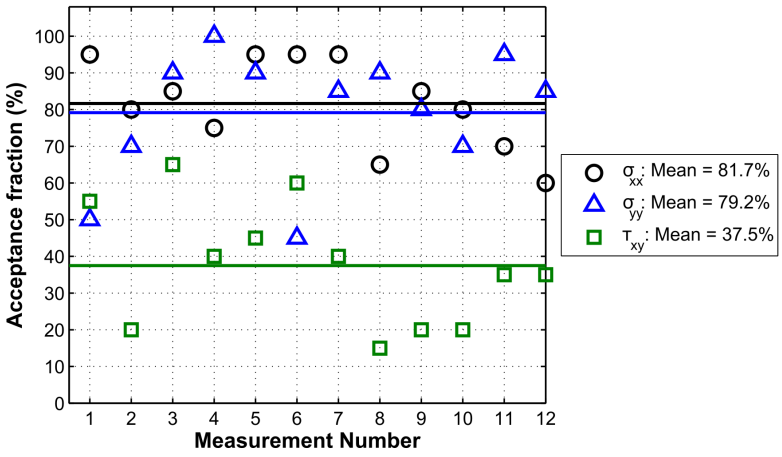

Fig. 9 – Acceptance fraction for each measurement in the shot peened titanium plate repeatability experiment

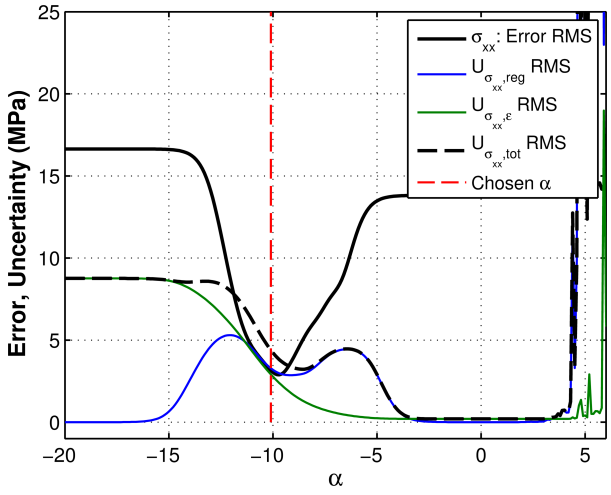

Fig. 10 – RMS regularization, strain, and total uncertainty and the RMS error for σ_{xx} as a function of α ($\alpha = \alpha_P = \alpha_Q = \alpha_T$) for the numerical experiment

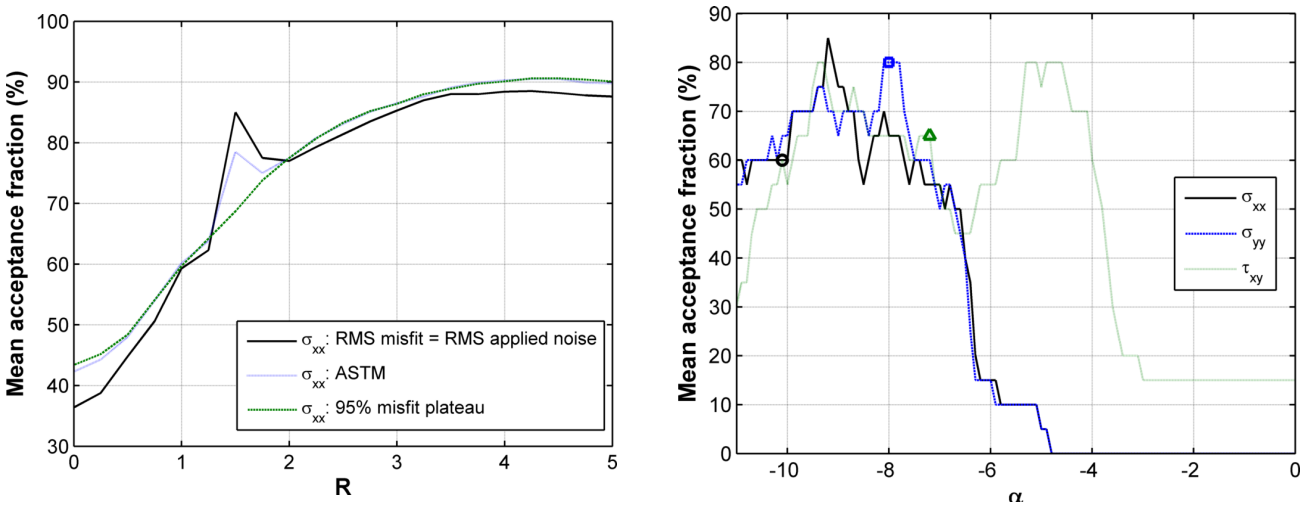

Fig. 11 – Mean acceptance fraction for (a) range of R values using a variety of α selection criterions and (b) vs. α (R=2) where the markers are at the misfit plateau

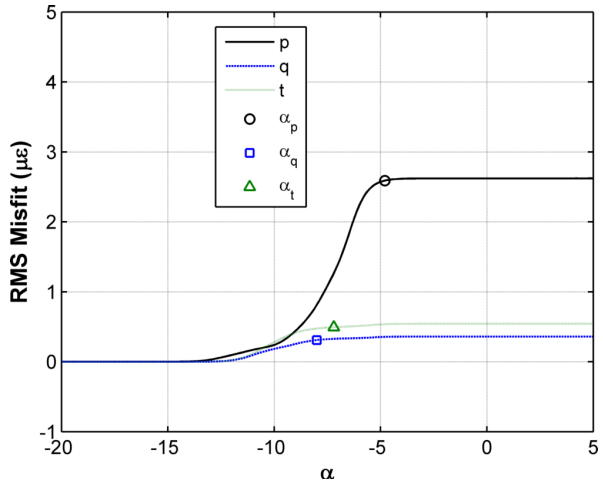

Fig. 12 – RMS misfit as a function of α for the numerical experiment. The markers show α values at 95% of the misfit plateau

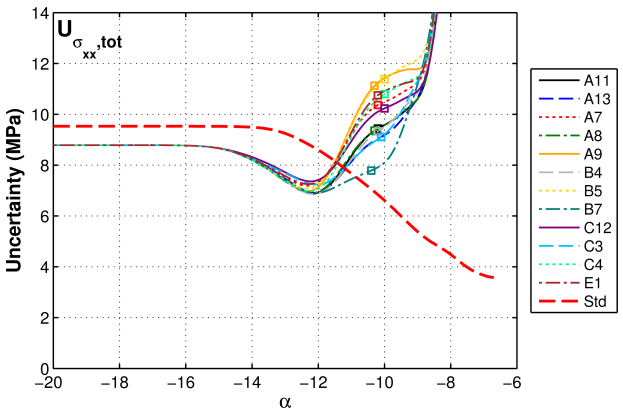

Fig. 13 – RMS total uncertainty and repeatability standard deviation for σ_{xx} in the shot peened aluminum plate vs α ($\alpha = \alpha_P = \alpha_Q = \alpha_T$)

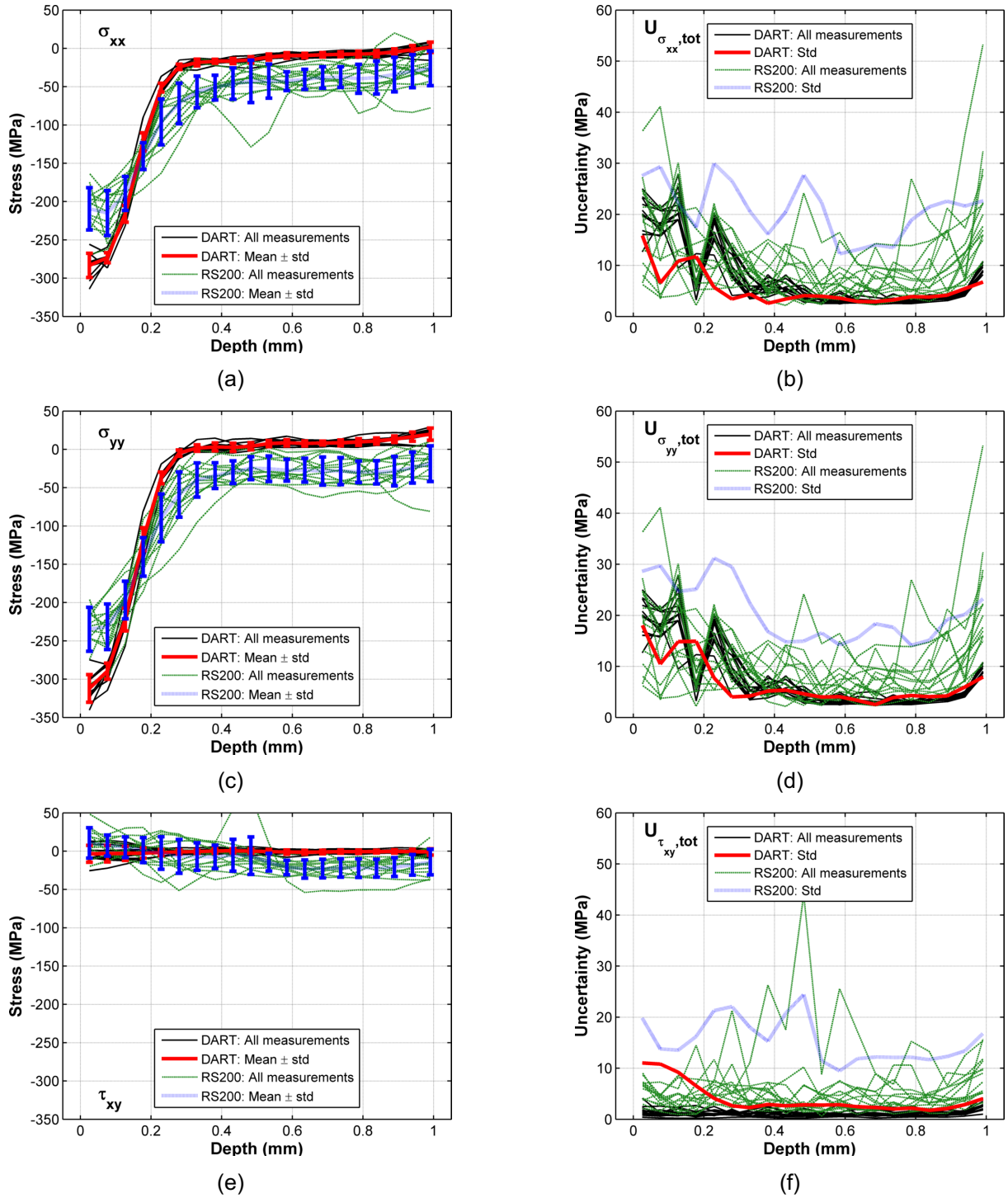

Fig. 14 – Repeatability data for the shot peened aluminum plate using the bespoke (DART) and RS200 milling machines. Calculated stress (and mean with the repeatability standard deviation shown as error bars) (left column) (a) σ_{xx}, (c) σ_{yy}, (e) τ_{xy} and uncertainty and repeatability standard deviation (right column) (b) σ_{xx}, (d) σ_{yy}, (f) τ_{xy}

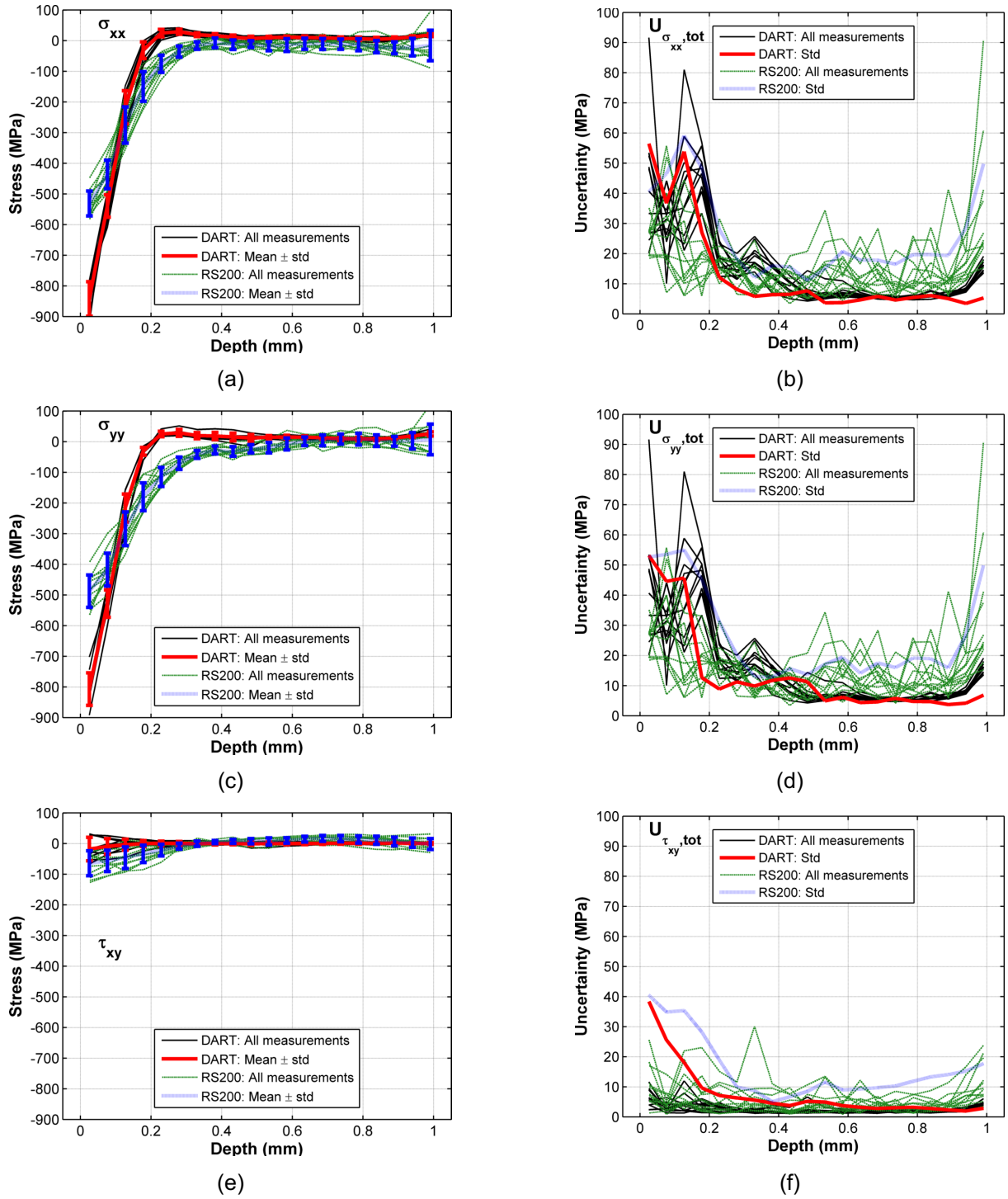

Fig. 15 – Repeatability data for the shot peened titanium plate using the bespoke (DART) and RS200 milling machines. Calculated stress (and mean with the repeatability standard deviation shown as error bars) (left column) (a) σ_{xx}, (c) σ_{yy}, (e) τ_{xy} and uncertainty and repeatability standard deviation (right column) (b) σ_{xx}, (d) σ_{yy}, (f) τ_{xy}